Ionic Strength Effect on Photochemistry of Fluorene and Dimethylsulfoxide at the Air-Sea Interface: Alternative Formation Pathway of Organic Sulfur Compounds in a Marine Atmosphere

The effect of halide ions on photochemistry of fluorene and DMSO at the air-sea interface: Alternative formation pathways of organic sulfur compounds in marine atmosphere

Majda Mekic[‡1,2], Jiafa Zeng[‡3], Wentao Zhou[1,2], Gwendal Loisel[1], Biao Jin[1], Xue Li[3], Davide Vione[4], Sasho Gligorovski[1*]

[1] State Key Laboratory of Organic Geochemistry, Guangzhou Institute of Geochemistry, Chinese Academy of Sciences, Guangzhou 510 640, China

[2]University of Chinese Academy of Sciences, Beijing 10069, China

[3]Institute of Mass Spectrometry and Atmospheric Environment, Jinan University, Guangzhou 510632, China

[4] Dipartimento di Chimica, Università di Torino, Via Pietro Giuria 5, 10125 Torino, Italy

Submitted to *ACS Earth and Space Chemistry*

*Corresponding author: gligorovski@gig.ac.cn

Abstract

The photochemical transformation processes occurring at the sea surface lead to the formation of low volatility organic compounds that contribute to new particle formation in the marine boundary layer (MBL). Here, we suggest an alternative formation pathway of organosulfur, halogenated and oxygenated aliphatic compounds, initiated by sunlight-activated fluorene (FL) and DMSO in the presence of the halide ions Cl^-, Br^-, and I^-. In particular, we observe a prompt formation of methanesulfonic acid (CH_3SO_3H, MSA) and methanesulfinic acid (CH_3SO_2H, MSIA), upon light irradiation of FL/DMSO. MSA and MSIA are typical precursors of secondary organic aerosols (SOA). We also show that the sunlight-initiated degradation of FL is considerably faster in the presence of halide ions, compared to its photochemical degradation in dilute aqueous phase. Therefore, the photochemical degradation of FL and potentially other PAHs would be faster in high ionic strength aerosol particles, compared to analogous diluted aqueous-phase photochemical processes occurring in, e.g., clouds. This could considerably affect the absorbing properties of the aerosols, which should be considered in future modeling studies.

Keywords: aerosol, biomass burning, photochemistry, ionic strength, UV-VIS spectroscopy

INTRODUCTION

The sea-surface microlayer (SSM) is defined as the uppermost 1 μm to 1 mm of the ocean surface that persists at wind speeds of up to 10 m s^{-1}.[1] The SSM is enriched with organic and inorganic compounds compared to the bulk aqueous phase. Both experimental and theoretical studies have demonstrated that halide ions are enhanced at the SSM, with enrichment in the order of $I^- > Br^- > Cl^-$ [2,3]. Dimethylsulfoxide (DMSO) is the most abundant organic sulfur compound at the SSM, deposited from the gas phase and produced by the photooxidation and bacterial degradation of dimethyl sulfide (DMS) [4-6]. For example, 78% of DMS in the aqueous phase is oxidized by ozone (O_3) to DMSO [7]. Long-term analyses of sea-surface samples collected in the period between 1995 and 2003 in the Arctic, Antarctica, Sub-polar North Atlantic, Sargasso Sea, Sub-tropical Atlantic, Mediterranean Sea, Black Sea, the coastal North Sea and the coastal Mediterranean Sea revealed that the DMSO concentrations range between 1 and 40 nM L^{-1} [5]. Despite its importance as an intermediate product of DMS oxidation, the behavior of DMSO has received relatively little attention.

Polycyclic aromatic hydrocarbons (PAHs) are ubiquitous in the SSM, arising from a variety of emissions. They are deposited from the gas phase to the ocean surface by air-water diffusive exchange, with concentrations ranging from 5 to 193 ng L^{-1} [8-12].The PAHs are enriched at the SSM due to their accumulation at the air-water interface [13-17]. For example, substantial concentrations of PAHs have been detected in the SSM, which were 200 to 400 times higher than in the sub-surface seawater collected in Chesapeake Bay.[18] Fluorene, pyrene and chrysene accounted for 77 % of the total amount of PAHs detected in the sea surface microlayer [18]. Fluorene (FL), a three-ring diaromatic hydrocarbon, exhibits concentrations in the range of 30 to 40 nM reaching up to ~50 nM at the SSM [13,19].

It has been shown that FL at the water surface can initiate photosensitized chemistry by its excited triplet state [26]. Although there are number of studies devoted to oxidation processes of PAHs in the gas phase and on various environmental surfaces,[20-25] the formation of secondary products is largely missing, especially in the gas phase. Grossmann et al.[27] have shown that the photodegradation of PAHs in different organic solvents is faster compared to their degradation in pure water [28].

There is scarce knowledge of the ionic strength effects on the photochemical degradation of organic compounds in the aqueous phase [29]. Recent studies have shown that ionic strength can affect the photochemical degradation of aqueous pyruvic acid, and also influence the reactive uptakes of ozone on pyruvic acid at a bromide-rich aqueous surface [30-32]. Comprehensive studies of the photochemical processes occurring at the SSM are required to improve our understanding of the ocean-atmosphere interactions [33].

In this study, for the first time to our best knowledge, we investigate the influence of halide ions (Cl^-, Br^-, and I^-) on the photochemical degradation of FL and DMSO, relevant for the upper sea surface. The gas-phase products formed during the photochemical degradation of FL and DMSO are assessed by the means of a secondary electrospray ionization high-resolution mass spectrometry (SESI-HR-MS). Many of the detected compounds can serve as precursors of secondary organic aerosols (SOA), which would add to the aerosol-formation pathways triggered by biological processes occurring in the ocean.

EXPERIMENTAL SECTION

Photoreactor for the kinetic studies

A custom-built double-wall photoreactor made up of borosilicate glass was used to assess the kinetics of the photochemical degradation of fluorene (FL) and dimethylsulfoxide (DMSO) at different salt concentrations [30,32]. The photoreactor is thermostated by thermostatic bath (LAUDA ECO RE 630 GECO, Germany). Fresh solutions of 1×10^{-4} mol L^{-1} FL (Sigma-Aldrich, 98%) were diluted in 100 mL of DMSO (Sigma-Aldrich, 98.5%) and sonicated until fully dissolved. Then, the freshly prepared solutions were mixed with ultrapure water (18.2 MΩ cm^{-1}, Sartorius, Germany) in the ratio 1:9 (FL+DMSO:H_2O). The resulting solutions were magnetically stirred during irradiation, and the temperature during all the experiments was held at 20°C.

The ionic strength of the solutions to be irradiated was adjusted by adding the required amount of sodium bromide (NaBr), sodium chloride (NaCl) and sodium iodide (NaI). All salts were purchased from Sigma Aldrich.

Photoreactor for the gas-phase product studies

To follow the formation of gas-phase products in the dark and upon irradiation of FL and DMSO, a double-wall rectangular photoreactor made up of borosilicate glass, with dimensions 5 x 5 x 2 cm was coupled to a secondary electrospray ionization high-resolution mass spectrometer (SESI-HRMS) [26]. The photoreactor is thermostated at 20°C by thermostatic bath (LAUDA ECO RE 630 GECO, Germany). An air flow of 200 mL min^{-1} (0-500 mL min^{-1} HORIBA METRON mass flow controller; accuracy, ±1%) was passed through the reactor during the experiments to bring

the formed gas-phase compounds through a 4 mm I.D. Teflon tube, into the stainless steel SESI chamber of the SESI-HRMS.

In order to solubilize FL (1×10^{-4} mol L^{-1}) (Sigma-Aldrich, 98%), a mixture of DMSO and ultrapure water (10:90 v/v), corresponding to a DMSO concentration of 1.4 mol L^{-1}, was used as solvent. We have chosen DMSO not only because it can help FL dissolution, but also because it is an abundant organic compound at the sea surface [6]. Similarly, high concentrations of the solvent have been used in previous work to study the solvent effect on PAHs photolysis [27], and it has been shown that organic solvents may affect PAH reactivity by changing the local environment [20,34]. The concentrations of NaCl, NaBr, and NaI in the reactor were 0.01 M, 0.001 M and 0.0001 M, respectively. The reactor was filled with 10 mL of freshly prepared solution. This experimental configuration was chosen to simulate calm seawater covered by an organic film made up of DMSO and FL, as a SSM proxy.

The pH of the FL/DMSO solution was measured using a pH meter (ORION STAR A326, Thermo Scientific, USA) to be 5.6 ± 0.03 before irradiation, and it increased to 7.3 ± 0.05 after 2 h of irradiation. All experiments were performed in duplicate.

For both types of photoreactors, a Xenon lamp (500 W) was used as a solar simulator to irradiate the solutions. A cutoff filter allowed for the transmission of UV-vis radiation in the wavelength range between 300 nm and 700 nm, which is relevant to the lower layer of the atmosphere close to the sea surface. The spectral irradiance was measured with a calibrated spectroradiometer (Ocean Optics, USA) equipped with a linear-array CCD detector, and compared to the sunlight radiation [35].

Secondary electrospray ionization high-resolution mass spectrometry (SESI-HRMS)

The gas-phase compounds formed upon irradiation of FL/DMSO were analyzed online and continuously by employing a homemade secondary electrospray ionization source coupled to a commercial Q Exactive Hybrid Quadrupole Orbitrap Mass spectrometer (Thermo Scientific, USA) [36]. In brief, a home-made Sec-nanoESI source was set up by integrating a commercial nano-ESI with a compact stainless steel chamber. The chamber was connected to the interface of the mass spectrometer. The flow of gas-phase compounds was consequently ionized by crossing with the nano-ESI plume in the ionization chamber. Ultrapure water (18.2 MΩ cm^{-1}, Sartorius, Germany) was used as ESI primary solvent. A 200 nL min^{-1} flow rate of ESI solvent was supplied with a nano-LC system (Thermo Scientific, USA). The temperature of the ion transfer capillary was held at 150 °C. The MS analyses were performed in the range *m/z* 50–500, at a resolution setting of 140 000 and a mass accuracy ≤ 2 ppm. The gas-phase samples were scanned in positive and negative ion detection modes, and the ESI voltage was set to 2.5 kV and −2.5 kV, respectively. Before starting the measurements, the mass spectrometer was calibrated with commercial standard solutions complying with the instructions of the manufacturer (Thermo Scientific, USA).

Data analysis. The raw data were pretreated by the Python program Breathfinder, developed by a collaborator (https://github.com/WanyangSun/BreathFinder). The information regarding the intensities of individual ions from each scan was extracted from the raw files. The data matrix was further investigated by using hierarchical cluster analysis and Kendrick Mass Defect (KMD) analysis,[37] which have been previously shown as suitable methodologies and have been widely used to show visualized trends in the elemental compositions of complex mixtures of organic

compounds in the atmosphere[38]. The possible element formula of a particular *m/z* signal was generated from Thermo Xcalibur (version 4.2.28.14, Thermo). HRMS has the capacity to distinguish low-intensity isobaric features and to accurately identify the elemental composition of unknown gas-phase compounds.

RESULTS AND DISCUSSION

Ionic strength effect on fluorene degradation kinetics

The pseudo first-order rate constants (k_{1st}) were obtained from the decay of FL as a function of the irradiation time at different salt concentrations. The concentrations of NaCl and NaBr varied in the range between 0 M and 1 M, and the concentration of NaI ranged between 0 M and 0.07 M. The experimental data were fitted with a three-parameter exponential function:

$$A_{\lambda_{max}}(t) = \alpha \cdot e^{-k_{1st} \cdot t} + \beta \qquad \text{(Eq-1)}$$

where $A_{\lambda_{max}}(t)$ is the absorbance at λ_{max} at the time t, α and β are fitting parameters, and k_{1st} is the pseudo first-order rate constant.

The k_{1st} value increased sharply by one order of magnitude, from $(2.1\pm0.1)\times10^{-4}$ s^{-1} at I = 0 M to $(2.1\pm0.2)\times10^{-3}$ s^{-1} at I = 0.1 M of NaCl. Then, the k_{1st} slightly decreased to $(1.5\pm0.04)\times10^{-3}$ s^{-1} at I = 0.5 M of NaCl. At higher ionic strength (I > 0.5 M) the value of k_{1st} decreased down to $(1.7\pm0.1)\times10^{-4}$ s^{-1} (Figure 1). In presence of NaBr, the k_{1st} increased by eight times, from $(2.1\pm0.1)\times10^{-4}$ s^{-1} at I = 0 M to $(1.6\pm0.2)\times10^{-3}$ s^{-1} at I = 0.3 M, and then slightly decreased to $(9.5\pm2.9)\times10^{-4}$ s^{-1} at I = 1 M. Similarly, in the presence of NaI the k_{1st} values increased by

almost one order of magnitude, from $(2.1\pm0.1)\times10^{-4}$ s^{-1} at I = 0 M to $(1.2\pm0.4)\times10^{-3}$ s^{-1} at I = 0.03 M, and then slightly decreased to $(8.5\pm0.5)\times10^{-4}$ s^{-1} at I = 0.07 M.

The increase of the pseudo first-order rate constants with increasing ionic strength can be described by the Debye-Huckel-Bronsted-Davies equation [32,39,40]:

$$\log k = \log k(I \to 0) + 2Z_A Z_B A \frac{\sqrt{I}}{1+\sqrt{I}} + b\, I \qquad \text{(Eq-2)}$$

where k is the observed pseudo first-order rate constant, A is the Debye-Hückel constant (A = 0.509 at 298 K), Z_A and Z_B are the absolute values of the charges for the involved species A and B, respectively, I is the ionic strength, and b is the kinetic salting coefficient.

In case of unimolecular reactions, as the direct photolysis of FL in the present case, the second term in Eq-2 can be neglected and the pseudo first-order rate constants depend on the empirical linear term (b · I), as follows:

$$\log k = \log [k(I \to 0)] + b\, I \qquad \text{(Eq-3)}$$

The kinetic salting coefficient (b) is an empirical parameter that depends on the difference between the activities of the reactant and the transition state [39]. The value of *b* determines the acceleration of the observed reaction in the presence of added salt [41,42]. Figure 1 shows that the observed pseudo first-order rate constants increase sharply with the ionic strength (0 < I <0.3 M for NaCl and NaBr, and 0 < I < 0.01 M for NaI), followed by a slight decrease at higher ionic strengths. In the case of NaCl, the observed pseudo first-order rate constant at I_{max} = 1 M approximately reached the initial k_{1st} value observed at I = 0 M.

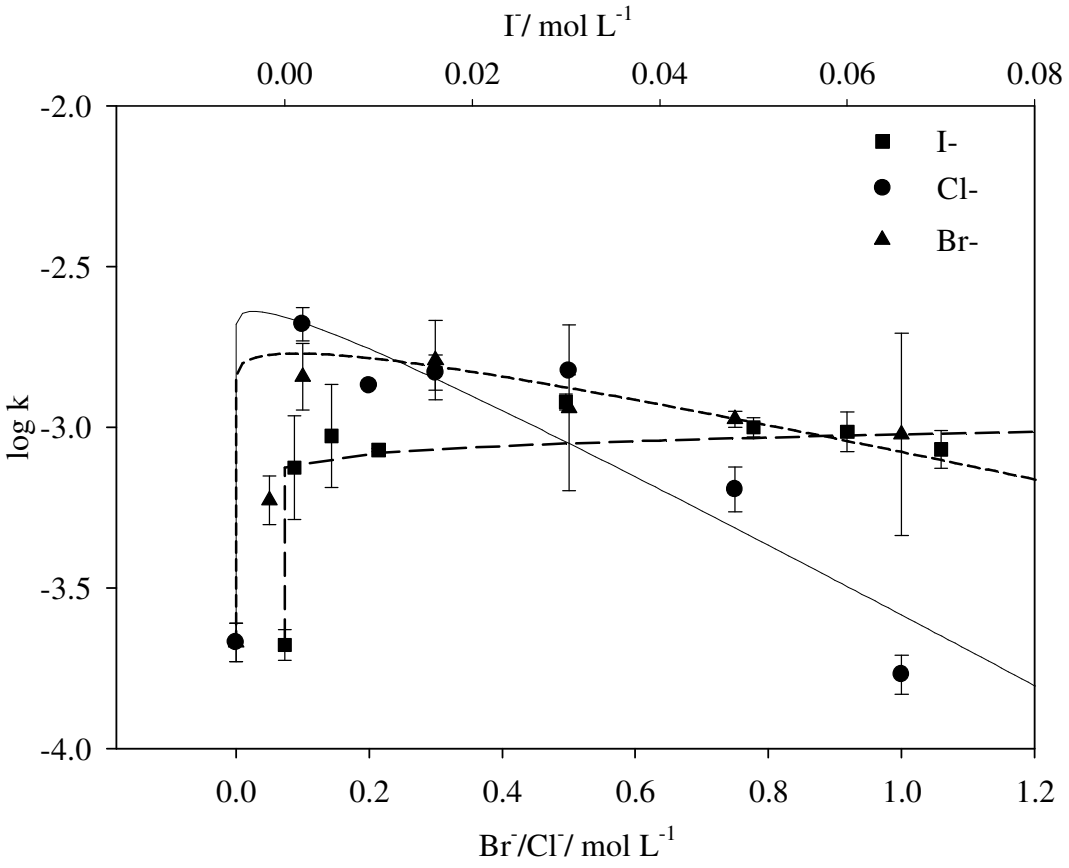

Figure 1. Trend of log k_{1st} vs. I at different concentrations of Cl^-, Br^-, and I^-. The error bars represent the σ-level uncertainty of the exponential data fit used to obtain k. The solid, short dash, and long dash lines represent the fit of the experimental data by Eq-4 for Cl^-, Br^- and I^-, respectively.

It has been suggested that higher-order empirical terms in Eq-3 could describe the slight decrease of the observed rate constants at higher ionic strength values, without any further physical insight [43]. Therefore, the hypothesis of Guggenheim was applied when modifying Eq-3 [32,44,45].

$$\log k = \log k(I \to 0) + A\frac{\sqrt{I}}{1+\sqrt{I}} + F_{ij}\, c_{ij} \qquad \text{(Eq-4)}$$

In Eq-4, F_{ij} is an adjustable kinetic parameter that depends on the solvent, the temperature and the nature of the ions *i* and *j*, and c_{ij} is the concentration of the supporting electrolyte. Figure 1 shows the fit of the observed pseudo first-order rate constants with Eq-4. The kinetic parameters F_{ij} emerging from the fit with Eq-4 are -1.16, -0.49, and 0.01 for NaCl, NaBr, and NaI, respectively. At low ionic strengths a catalytic effect of the Cl^-, Br^-, and I^- ions leads to a sharp linear increase of the rate constants, in agreement with previous studies focused on ionic strength effects on reaction rate constants in the atmospheric aqueous phase [46,47]. The negative values of F_{ij} for Cl^- and Br^- predicted by the fit indicate the decreasing degradation rates of FL at higher Cl^- and Br^- concentrations, while $F_{ij} = 0.01$ indicates a very slow (almost plateau) increase of the degradation rate of FL at higher I^- concentrations. The second-order rate constants for bimolecular reactions of atmospheric relevance exhibited similar behavior at higher ionic strengths [40,43,48,49]. Obviously, the ionic strength affects the photochemical degradation of FL and possibly other PAHs enriched at the sea surface and in the marine aerosol particles, a fact that should be considered in future modeling studies.

Formation of gas-phase products

Cluster analysis. The presence of FL and DMSO that would be enriched at the surface of synthetic seawater containing Cl^-, Br^- and I^-, in the dark and under simulated sunlight irradiation, can initiate different chemical pathways of VOCs formation. As a result, many VOCs were detected by SESI-HRMS and were further grouped into separated clusters. A total of 334 ions with intensities $\geqslant 1 \cdot 10^5$ a.u. were detected in real-time by SESI-HRMS, and analyzed by the Clustergram function in Matlab R2014b. Five groups of ions in the dark and under irradiation, illustrating different chronological variations, are shown in Figure 2. In general, the detected ions

under both experimental conditions (Figure 2 A and B) could be divided in different groups according to their distinguished features and time-resolved profiles.

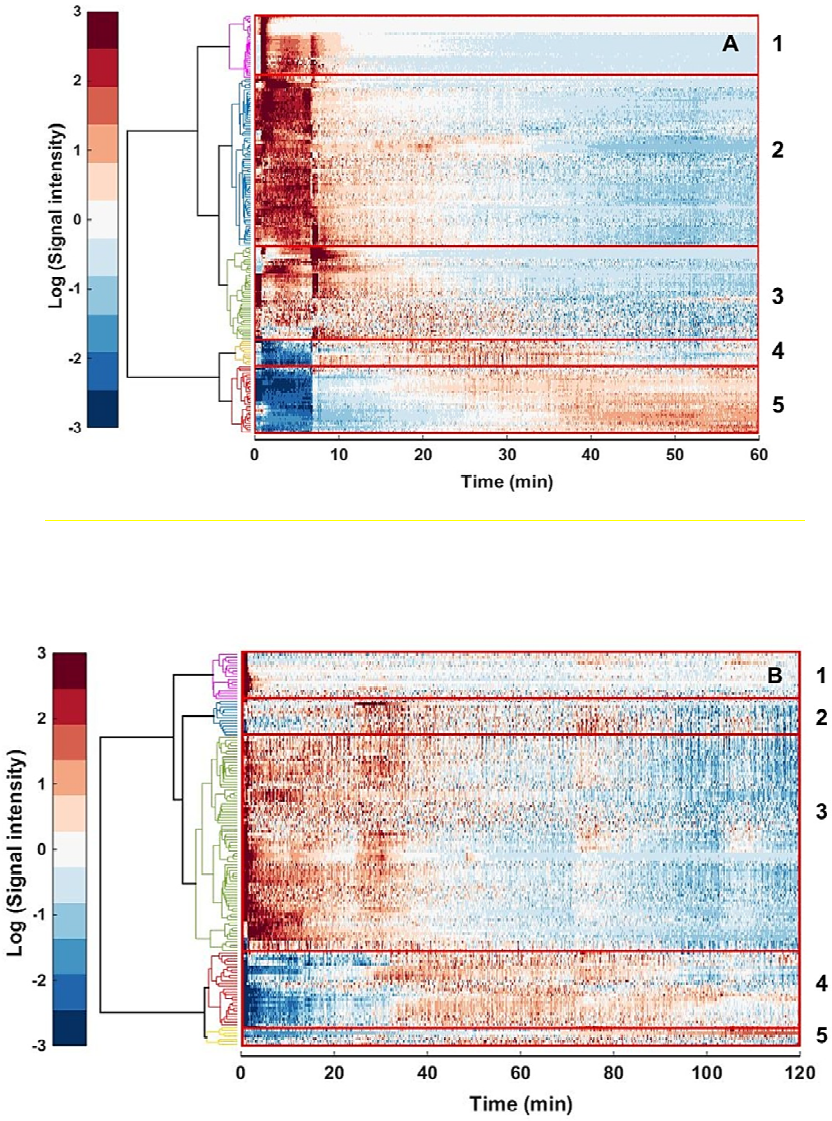

Figure 2: Cluster analysis of 334 ions with intensities ≥ $1 \cdot 10^5$ a.u. in the dark (A) and under light irradiation (B), respectively. Different chronological variations of the formed VOCs were identified and separated into five different groups, under both experimental conditions (A and B).

For example, on both graphs, the first three groups contain ions, the intensities of which start decreasing after 5 min. In contrast, the features in the last two clusters (5 and 6) are characterized by the fact that the ions reach the maximum peak level 25 min after the reaction has started.

Most of the halogen-containing oxidized compounds (CHOX, with X=Cl, Br, I) were identified in group 1 (29 ions), and they were mostly formed within the first 5 min of the reaction. Features in group 2 (80 ions) and group 3 (45 ions) exhibited a similar trend, with the maximum intensity reached in the first 5 min of the reaction. The observed tendency of the products with high intensities continued up to 30 min after the start of the reaction. Based on the chemical composition of most ions from groups 2 and 3, we conclude that these two groups mainly consist of saturated long chain fatty-acids. In addition, when compounds from group 4 (12 ions) and group 5 (32 ions) were formed, the intensities of the other compounds from groups 1-3 were already dramatically reduced. Hence, the ions from groups 4 and 5 might be described as secondary products from the self-reaction of FL and the reaction of FL with DMSO. The identified chemical compositions suggest that most of the ions in group 4 might be oxidized products with 3 to 4 oxygen atoms and DBE (Double-Bond equivalents) ranging between 2.5 and 3.5. The products identified in group 5 are sulfur-containing oxidized compounds (CHOS). Most of these CHOS compounds contain only one sulfur atom, with low DBE values (0.5-1).

Most of the ions detected under light irradiation of the mixture FL/DMSO exhibit similar time evolution profiles (Figure 2B) as the ions generated under dark conditions (Figure 2A). Similarly, group 1 (17 ions) might be classified as sulfur-containing compounds (CHOS) with only one sulfur atom in their chemical structures. More importantly, 11 out of the 17 identified ions in this group are new ions, in the sense that they appeared solely in presence of light. Most of the ions in group 2 (11 ions) increased 30 min after light exposure of the solution, indicating formation of

halogenated organic compounds (CHOX). The most numerous cluster is group 3 with 115 ions, mostly consisting of oxygenated long-chain molecules with up to 18 carbon atoms and DBE values ranging from 1.5 to 2.5. It is evident from Figure 2B that the majority of the classified ions in this group appeared in the first 30 min from the beginning of the light-induced process. In analogy with Figure 2A, the last two groups (group 5 and group 6) of Figure 2B did not form at the beginning of the experiment but they started appearing after 30 min of continuous light irradiation. Thus, ions from group 5 (26 ions) and group 6 (7 ions) might be regarded as secondary products initiated by the excited triplet state of FL [26] and DMSO. Regarding the elemental composition of identified ions from group 5, they are mostly sulfur-containing organic compounds (CHOS), while those of group 6 are likely to be oxygenated compounds (CHO).

Kendrick Mass Defect (KMD) analysis. The molecular composition of the compounds was calculated with Xcalibur and using KMD analysis, to find out the homologous compounds differing only by the number of a base unit CH_2 group. Figure 3 illustrates the KMD plot for all the observed ions under dark (A) and light-initiated (B) conditions. The KMD diagram is usually used for finding relationships between large dataset of molecular formulas, provided by ultra-high resolution mass spectrometry (UHRMS) studies [36,50,51]. Here, the regular space pattern of CH_2 was fixed at precisely 14 u and was used as the reference mass for calculating the Kendrick mass (KM), expressed in Eq-5.

$$KM\ (CH_2) = \text{observed mass} \cdot (14.00000/14.01565) \quad \text{(Eq-5)}$$

In contrast, the KMD is defined as the difference between nominal mass, obtained as rounding the number to the nearest integer, and KM as given by Eq-6.

$$KMD\ (CH_2) = \text{nominal mass (NM)} - KM \quad \text{(Eq-6)}$$

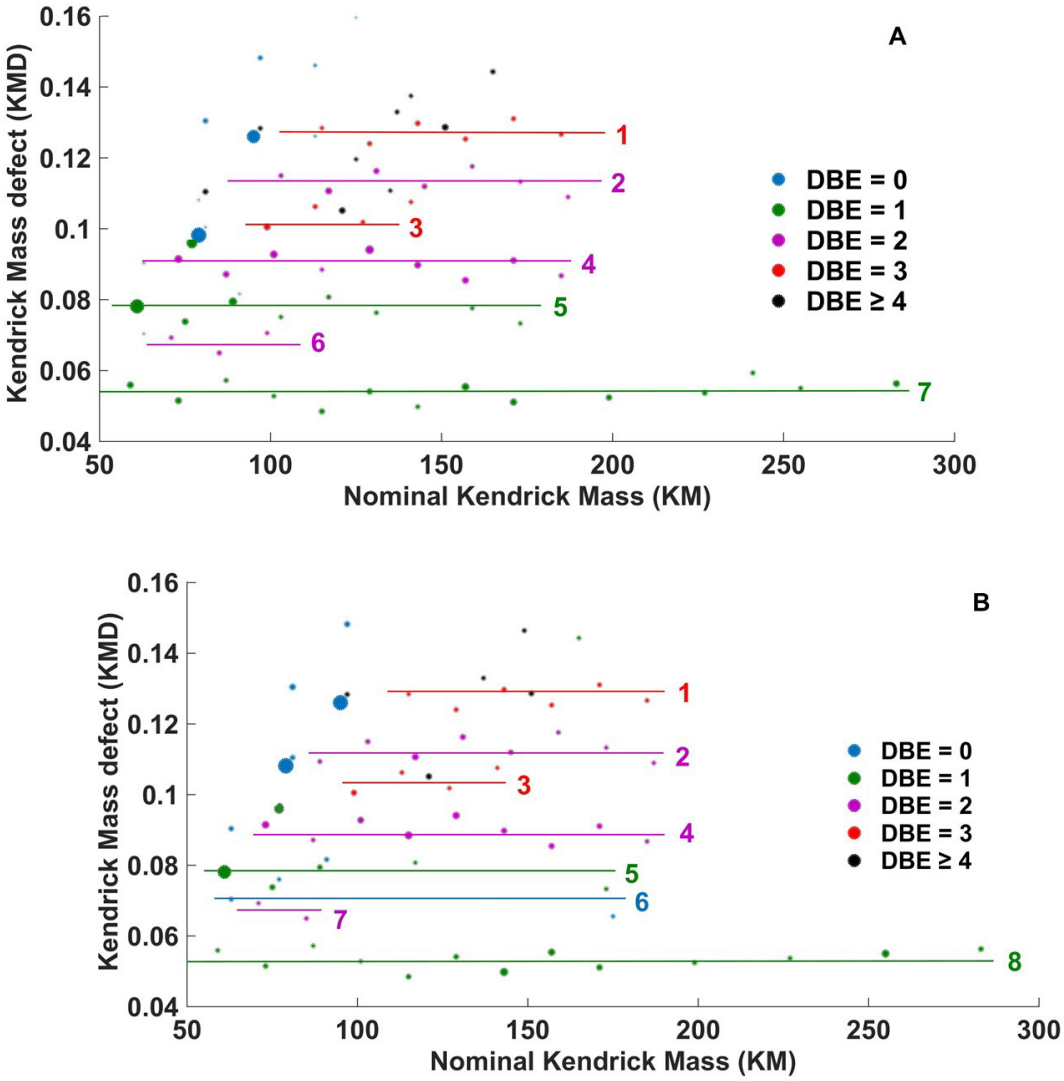

Figure 3: CH_2-based Kendrick mass defect diagram of all *m/z* values of identified ions in negative ion detection mode, under dark (A) and irradiated (B) conditions, respectively. The solid lines connect the compounds, which differ from each other only by an integer number of CH_2 groups and thus, belong to the same homologous series. For example, the homologues series on the graph A might be expressed as Line 1: $C_nH_{2n-4}O_4$, Line 2: $C_nH_{2n-2}O_4$, Line 3: $C_nH_{2n-4}O_3$, Line 4: $C_nH_{2n-2}O_3$, Line 5: $C_nH_{2n}O_3$, Line 6: $C_nH_{2n-2}O_2$, Line 7: $C_nH_{2n}O_2$. On graph B, Line 1: $C_nH_{2n-4}O_4$, Line 2: $C_nH_{2n-2}O_4$, Line 3: $C_nH_{2n-4}O_3$, Line 4: $C_nH_{2n-2}O_3$, Line 5: $C_nH_{2n}O_3$, Line 6: $C_nH_{2n+2}OS$, Line 7: $C_nH_{2n-2}O_2$, Line 8: $C_nH_{2n}O_2$, respectively. The size of symbols is proportional to the abundance of the ions. The color-coding indicates the calculated DBE values.

After this estimation all identified ions, which differ only in the number of the used regular spacing pattern, fall on the same horizontal lines in the KMD plot and belong to the same homologous series (Figure 3). Such series are defined here as CH_2-based KMD patterns, and all compounds of a homologous series exhibit the same DBE (this value is also added on the graph as color-coding). DBEs, which correspond to the sum of double bonds and rings in molecules, were estimated as:

$$DBE = c - (h/2) + (n+2) + 1 \quad \text{(Eq-7)}$$

assuming only compounds with a general formula $C_cH_hN_nO_oS_s$.

In negative mode, we identified within the CHO sub-group 7 (dark) and 8 (light) homologous series, composed of 2 to 14 compounds, differing only in mass of CH_2. Moreover, as a result of the used KMD analysis, there was 1 CHOS homologous series identified under irradiation conditions. However, it is worth noting that although the compounds lie on the same homologous series, they are not necessarily structurally related but they are only associated with similar elemental composition [52].

KMD (CH_2) series 1 appeared under both experimental conditions (dark and light) and might be characterized with the formula $C_nH_{2n-4}O_4$. In both cases, the series starts with the tentatively identified compound $C_4H_4O_4$, possibly 2-butenedioic acid, and it contains six members up to C9, which might be attributed to unsaturated dicarboxylic acids. They could be assigned also as diketo-monocarboxylic acids, having a DBE value of 3.

Series 2, which has been tentatively identified as long-chain dicarboxylic acids with a general formula of $C_nH_{2n-2}O_4$ for the homologous series, most likely starts with oxalic acid ($C_2H_2O_4$) in

the dark, and with its C3 analogue under irradiation. In both cases (dark and light) it contains seven (Fig. 3B) to eight (Fig. 3A) members, up to C8, which all show a DBE of 2.

Series 3 is illustrated with a tentatively developed formula of $C_nH_{2n-4}O_3$. It can be seen from both graphs (Fig. 3A and 3B) that within this series, 4 compounds are produced under our experimental conditions and have a DBE of 3. The series starts with m/z 99.01 ($C_4H_4O_3$), which might be most probably attributed to unsaturated hydroxyl dialdehydes or diketones.

Series 4, both in the dark and under irradiation, can be described with the general formula $C_nH_{2n-2}O_3$. Most formulae within this series have a DBE value of 2, and might be tentatively characterized as unsaturated hydroxyl monocarboxylic acids, saturated anhydride or keto/oxo esters. The formula $C_2H_2O_3$ in this series may most likely correspond to oxo-acetic acid with m/z 72.99, making it the smallest compound of the series. Some larger compounds of this series have up to C10, where the largest member shows the formula $C_{10}H_{18}O_3$ and m/z 185.12.

The identified series 5 exhibits a low DBE value of 1, and could be summarized with the general formula $C_nH_{2n}O_3$. The smallest compound is probably CH_2O_3 with m/z 60.99, while the largest member's in this series had m/z 159.10 with a formula of $C_8H_{16}O_3$. All members of series 5 might be tentatively identified as hydroxy carboxylic acids, hydroxyl esters or dihydroxy aldehydes.

Members of a further series, characterized by the general formula $C_nH_{2n-2}O_2$ and a DBE of 2 (number 6 in dark and 7 under photolysis), could be unsaturated monocarboxylic acids. Both series with two (Fig. 3B) and three (Fig. 3A) members, respectively, start with acrylic acid ($C_3H_4O_2$). In both cases, the small number of members and the very limited length of the homologous series suggests that the formation of unsaturated monocarboxylic acids is not that

significant in the analyzed samples, despite the fact that they are widespread in the environment [52,53].

The only group, which appeared solely under irradiation (series 6) is the sulfur-containing subgroup. Here, the majority of the identified formulae contain only one sulfur atom and exhibit a low degree of oxidation and unsaturation. Moreover, these OS compounds are characterized by long aliphatic carbon chains. The smallest CHOS compound, found in this CH_2 reference mass of KMD series, is probably methanesulfenic acid (CH_4OS). This series contains only two members, which is not surprising because it is usually found that series having heteroatoms such as N or S are way shorter than those composed of only CHO compounds [52]. Long-chain OS have been found in different field measurements across several locations in China. These aliphatic-like sulfur-containing compounds might affect the hygroscopicity of the formed particles, and consequently impact their surface tension [54].

The longest of all CH_2 series with 14 (line 7 in the dark) or 13 members (line 8 under irradiation conditions) could be illustrated as saturated long-chain alkanoic acids, having DBE of 1. The smallest member of this series is $C_2H_3O_2$ with *m/z* 59.01, which might be acetic acid, and the largest member of the series corresponds to *m/z* 283.26 with molecular composition of $C_{18}H_{36}O_2$, possibly representing octadecanoic acid.

Time evolution of organic sulfur compounds under light irradiation

The chemical interaction between FL and DMSO, in the dark and under light irradiation, releases a broad variety of unsaturated multifunctional, organosulfur and even halogenated compounds in

the gas phase. Figure 4 shows typical time evolution profiles of organic sulfur compounds in the gas phase, under irradiation of FL and DMSO in the presence of halide ions.

Upon light irradiation of FL/DMSO, we observed prompt formation in the gas phase of methanesulfonic acid (CH_3SO_3H, MSA), methanesulfinic acid (CH_3SO_2H, MSIA), hydroxymethanesulfonic acid (CH_4O_4S, MSAOH), and 2-hydroxyethenesulfonic acid ($C_2H_5O_4SH$, ESAOH). These compounds are typical precursors of aerosol particles, and they are commonly detected in ambient particles [55,56].

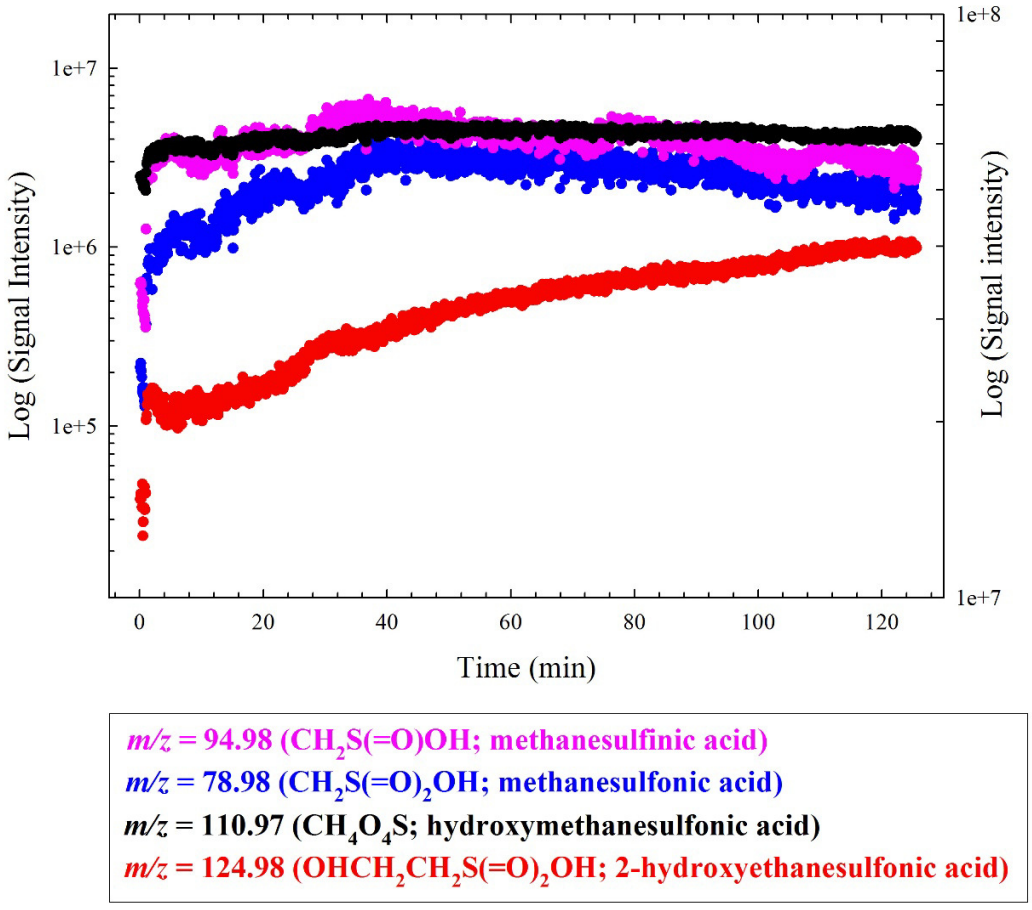

Figure 4: Time profiles (SESI-HRMS) of the selected ions under light conditions. All ions are scanned in ESI- and exhibit intensities $\geq 1 \cdot 10^5$ a.u.

The photochemical model described below provides insight into the possible environmental significance of this process, and shows the formation rates of these organic sulfur compounds throughout the year under environmentally relevant conditions.

Photochemical model

The formation rate R_F of a reaction product upon irradiation of FL + DMSO can be expressed by Eq-8, where k_F is the first-order formation rate constant of the product, C_o the initial concentration of FL, P_a the photon flux absorbed by FL, Φ_F the quantum yield of product formation, $p°(\lambda)$ the incident spectral photon flux density of the lamp, $\varepsilon_{FL}(\lambda)$ the molar absorption coefficient of FL at the wavelength λ, and b the optical path length in the photoreactor (1 cm):

$$R_F = k_F C_o = \Phi_F P_a = \Phi_F \int_\lambda p°(\lambda)[1-10^{-\varepsilon_{FL}(\lambda)bC_o}]d\lambda \quad \text{(Eq-8)}$$

Because the absorbance of FL ($\varepsilon_{FL}(\lambda)bC_o$) in the photoreaction system is relatively low, the exponential equation used for the calculation of the absorbed photon flux can be approximated as follows:

$$1-10^{-\varepsilon_{FL}(\lambda)bC_o} \approx 2.3\varepsilon_{FL}(\lambda)bC_o \quad \text{(Eq-9)}$$

Therefore, the following relationship holds for R_F that allows for directly linking k_F and Φ_F:

$$R_F = k_F C_o = 2.3bC_o \Phi_F \int_\lambda p°(\lambda)\varepsilon_{FL}(\lambda)d\lambda \quad \text{(Eq-10)}$$

It is thus possible to calculate Φ_F from the experimental values of k_F:

$$\Phi_F = \frac{k_F}{2.3 b \int_{\lambda} p°(\lambda)\,\varepsilon_{FL}(\lambda)\,d\lambda} \qquad \text{(Eq-11)}$$

The following table reports the calculated values of Φ_F for the different compounds that were experimentally monitored (MSA: methanesulfonic acid; MSIA: methanesulfinic acid; MSAOH: hydroxymethanesulfonic acid; ESAOH: hydroxyethanesulfonic acid). These values represent the overall quantum yields of the process that encompasses both the liquid-phase formation of the reaction products, and their transfer from the liquid to the gas phase.

Table 1. Formation rate constants and quantum yields of sulfur-containing compounds, detected in the gas phase upon irradiation of FL/DMSO.

Compound	k_F (s^{-1})	Φ_F (unitless)
MSA	3.3×10^{-5}	0.16
MSIA	3.5×10^{-5}	0.17
MSAOH	9.0×10^{-5}	0.43
ESAOH	4.5×10^{-5}	0.21

From the values of Φ_F, it is possible to model the kinetics by which the detected compounds could reach the gas phase upon sunlight irradiation of FL + DMSO in the sea surface layer. Considering that FL can reach 50 nM concentration [13] in a layer of 1 mm thickness, the low-absorbance approximation also holds in the environmental scenario. Therefore, by rearranging Eq-11, the formation rate constant of the intermediate can be expressed as follows:

$$k_F = 2.3\ \Phi_F\ b \int_{\lambda} p°(\lambda)\,\varepsilon(\lambda)\,d\lambda \qquad \text{(Eq-12)}$$

where b = 0.1 cm (*i.e.*, the 1 mm microlayer thickness), and $p°(\lambda)$ is the incident spectral photon flux density of sunlight at the water surface. Figure 5 reports the values of k_F for the various intermediates in different months of the year, calculated for average sunlight at 50°N latitude. The considerable difference between summer and winter formation kinetics is accounted for by the fact that FL mostly absorbs UVB sunlight. The sunlight spectra used as $p°(\lambda)$ [57] are reported in figure 6, and represent daylight-averaged spectra for the given month and latitude.

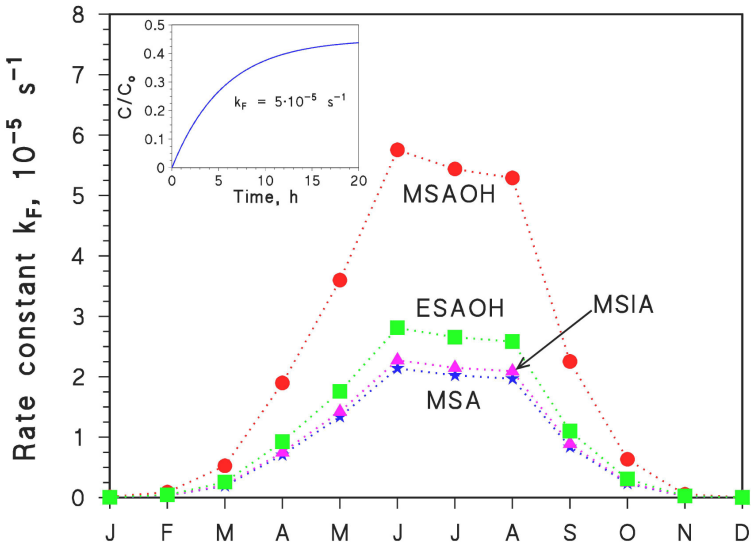

Figure 5: Modelled photochemical formation rate constants (k_F) of MSA, MSIA, MSAOH and ESAOH in different months of the year, at 50°N latitude. The figure insert shows the modelled formation trend of MSAOH when $k_F = 5 \cdot 10^{-5}$ s^{-1}, under the hypothesis that 100% FL is transformed into MSAOH, ESAOH, MSA and MSIA. In this scenario, MSAOH would account for 45% of the reaction products. Note that C is the concentration of MSAOH, while C_o is the initial FL concentration.

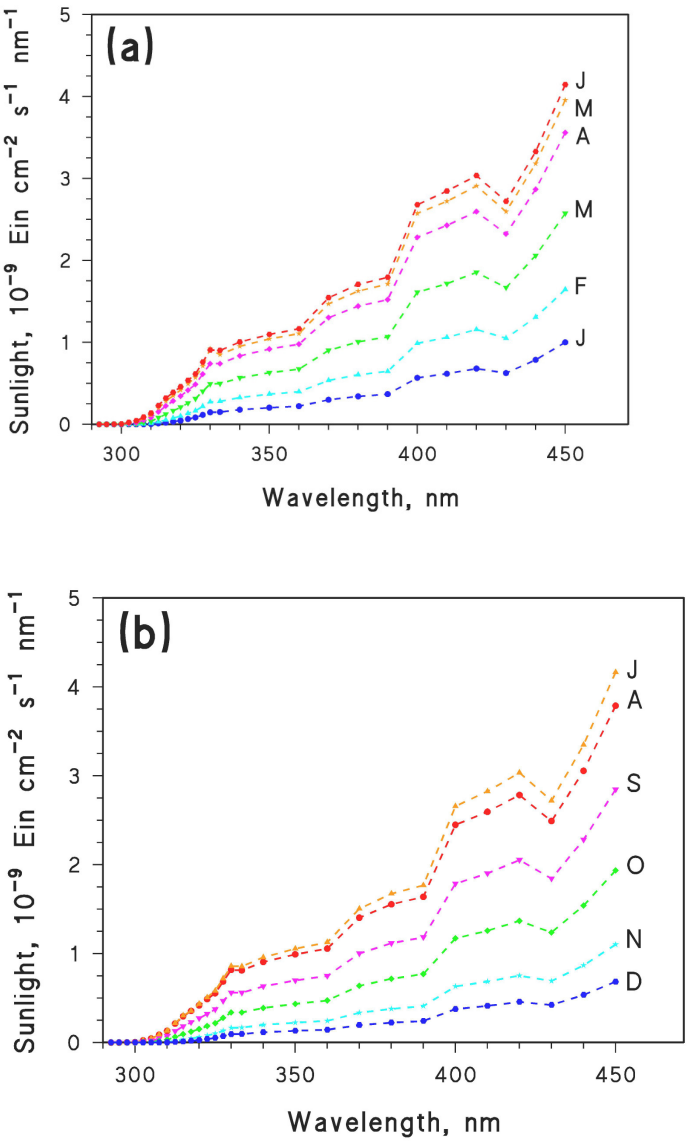

Figure 6: Sunlight $p°(\lambda)$ values in different months of the year at 50°N latitude, used for photochemical modelling. (a): January to June; (b) July to December.[57]

In obvious agreement with the experimental findings, MSAOH is the compound that would reach the most the gas phase. Interestingly, during the summer months one expects significant MSAOH formation in just a few hours under fair-weather conditions (see the insert of Figure 5), which makes the photochemical process potentially significant. It should be remarked that the total amount of MSAOH formed is limited by the concentration of FL at the air-water interface (C_o in the figure insert).

CONCLUSIONS

The kinetics of FL photodegradation was dramatically enhanced in presence of low concentrations of halide ions (0.1 M for Cl^- and Br^-, and 0.001 for I^-), compared to photodegradation without halides. In the case of Cl^- and Br^- the FL photodegradation kinetics reached a maximum when increasing the halide concentration, while with I^- the overall increasing trend reached a plateau. Hence, the photochemical degradation of FL enriched at the sea surface or in marine aerosol particles could proceed with much faster kinetics, compared to the photochemical transformation of FL in the dilute aqueous phase (cloud, fog) at low levels of halide ions. The PAHs buried in aerosol particles account for only 7% of the total organic aerosol mass, but due to their light-absorbing properties, they contribute up to ca. 40% of the total absorbance of aerosol particles (Lu et al., 2015). Therefore, relatively fast photochemical degradation of FL and potentially other PAHs in halide-rich aerosol particles could considerably affect the absorbing properties of the aerosols. This feature of PAHs in atmospheric aerosol deliquescent particles should be considered in future modeling studies.

The different kinetics between the dilute aqueous phase and concentrated salt solutions can affect the formation of secondary products in the gas phase. The photochemical transformation of

FL/DMSO in simulated saltwater yielded large amounts of oxygenated, aliphatic, aromatic, organic halogen and organic sulfur compounds. The only known source of MSA and MSIA in the marine atmosphere is the oxidation of DMS, which is produced biologically by oceanic phytoplankton in the oceans. This study reports direct evidence of MSA and MSIA production from the photochemical degradation of FL/DMSO. The photochemical conversion of DMSO into MSA and MSIA, initiated by light-excited FL, provides an alternative formation pathway of OS compounds in the marine boundary layer.

The oxygenated long-chain aliphatics and the OS compounds produced by the photochemical oxidation of PAHs and DMSO can participate in SOA formation, which in turn can better explain field observations of new particle formation events which are occurring independently of the primary emitted particles from biological activity in the sea (O'Dowd et al., 2004).

AUTHOR INFORMATION

Corresponding Author

*Sasho Gligorovski

e-mail: gligorovski@gig.ac.cn

Author Contributions

The manuscript was written through contributions of all authors. All authors have given approval to the final version of the manuscript. ‡These authors contributed equally.

ACKNOWLEDGMENT

(This study was financially supported by the National Natural Science Foundation of China (41773131, and 41977187). We are grateful to Guangdong Foundation for Program of Science and Technology Research, Grant N°: 2017B030314057.

ABBREVIATIONS

FL, Fluorene, DMSO, Dimethylsulfoxide, SESI-HRMS, Secondary electrospray ionization high resolution mass spectrometry

REFERENCES

1. Wurl, O.; Werner, E.; Landing, W. M.; Zappa, C. J. Sea surface microlayer in a changing ocean – A perspective. *Elementa-Sci. Anthrop.* **2011**, *5*, 31-42.
2. Jungwirth, P.; Tobias, D. J. Specific Ion Effects at the Air/Water Interface. *Chem. Rev.* **2006**, *106*, 1259-1281.
3. Carpenter, L. J.; Nightingale, P. D. Chemistry and Release of Gases from the Surface Ocean. *Chem. Rev.* **2015**, *115* (10), 4015-4034.
4. Legrand, M.; Sciare, J.; Jourdain, B.; Genthon, C. Subdaily variations of atmospheric dimethylsulfide, dimethylsulfoxide, methanesulfonate, and non-sea-salt sulfate aerosols in the atmospheric boundary layer at Dumont d'Urville (coastal Antarctica) during summer. *J. Geophys. Res.* **2011**, *106*, 14409-14422.
5. Simo, R.; Vila-Costa, M. Ubiquity of algal dimethylsulfoxide in the surface ocean: geographic and temporal distribution patterns. *Mar. Chem.* **2006**, *100*, 136-146.
6. González-Gaya, B.; Fernández-Pinos, M-C.; Morales, L.; Méjanelle, L.; Abad, E.; Piña, B.; Duarte, C.M.; Jiménez, B.; Dachs, J. High atmosphere–ocean exchange of semivolatile aromatic hydrocarbons. *Nat. Geosci*. **2016**, *9*, 438–442.
7. Hoffmann, E. H.; Tilgner, A.; Schrödner, R.; Bräuer, P.; Wolke, R.; Herrmann, H. An advanced modeling study on the impacts and atmospheric implications of multiphase dimethyl sulfide chemistry. *Proc. Natl. Acad. Sci. U. S. A.* **2016**, *113*, 11776-11781.
8. Pérez-Cerrera, E.; León, V. M.; Parra, A. G.; González-Mazo, E. Simultaneous determination of pesticides polycyclic aromatic hydrocarbons and polychlorinated biphenyls in seawater and interstitial marine water samples, using stir bar sorptive

extraction-thermal desorption-gas chromatography-mass spectrometry. *J. Chromatogr. A* **2007**, *1170*, 82–90.
9. Valavanidis, A.; Vlachogianni, T.; Triantafillaki, S.; Dassenakis, M.; Androutsos, F.; Scoullos, M. Polycyclic aromatic hydrocarbons in surface seawater and in indigenous mussels (Mytilus galloprovincialis) from coastal areas of the Saronikos Gulf (Greece), *Estuar. Coast. Shelf S.* **2008**, *79*, 733–739.
10. Ma, Y.; Xie, Z.; Yang, H.; Möller, A.; Halsall, C.; Cai, M.; Sturm, R.; Ebinghaus, R. Deposition of polycyclic aromatic hydrocarbons in the North Pacific and the Arctic. *J. Geophys. Res. Atmos*. **2013**, *118*, 5822–5829.
11. Otto, S.; Streibel, T.; Erdmann, S.; Klingbeil, S.; Schulz-Bull, D.; Zimmermann, R. Pyrolysis–gas chromatography–mass spectrometry with electronionization or resonance-enhanced-multi-photon-ionization for characterization of polycyclic aromatic hydrocarbons in the Baltic Sea. *Mar. Pollut. Bull.* **2015**, *99*, (1-2), 35-42.
12. González-Gaya, B.; Martínez-Varela, A.; Vila-Costa, M.; Casal, P.; Cerro-Gálvez, E.; Berrojalbiz, N.; Lundin, D.; Vidal, M.; Mompeán, C.; Bode, A.; Jiménez, B.; Dachs, J. Biodegradation as an important sink of aromatic hydrocarbons in the oceans. *Nat. Geosci.* **2019**, *12*, 119–125.
13. Cincinelli, A.; Stortini, A. M.; Perugini, M.; Checcjini, L.; Lepri, L. Organic pollutants in sea-surface microlayer and aerosol in the coastal environment of Leghorn—(Tyrrhenian Sea). *Mar. Chem.* **2001**, *76*, 77-98.
14. Vacha, R.; Jungwirth, P.; Chen, J.; Valsaraj, K. Adsorption of polycyclic aromatic hydrocarbons at the air–water interface: molecular dynamics simulations and experimental atmospheric observations. *Phys. Chem. Chem. Phys.* **2006**, *8*, 4461-4467.
15. Chen, J.; Ehrenhauser, F. S.; Valsaraj, K. T.; Wornat, M. J. Uptake and UV-photooxidation of Gas-phase PAHs on the Surface of Atmospheric Water Films. 1. Naphthalene. *J. Phys. Chem. A.* **2006**, *110*, 9161-9168.
16. Lohmann, R.; Gioia, R.; Jones, K. C.; Nizzetto, L.; Temme, C.; Xie, Z.; Schulz-Bull, D.; Hand, I.; Morgan, E.; Jantunen, L. Organochlorine Pesticides and PAHs in the Surface Water and Atmosphere of the North Atlantic and Arctic Ocean. *Environ. Sci. Technol.* **2009**, *43*, 5633-5639.
17. Seidel, M.; Manecki, M.; Herlemann, D.P.R.; Deutsch, B.; Schulz-Bull, D.; Jürgens, K.; Dittmar T. Composition and Transformation of Dissolved Organic Matter in the Baltic Sea. *Front. Earth Sci.* **2017**, *5*, *(31)* doi: 10.3389/feart.2017.00031.
18. Hardy, J. T.; Crecelius, E. A.; Antrim, L. D.; Kiesser, S. L.; Broadhurst, V. L. Aquatic Surface Microlayer Contamination in Chesapeake Bay. *Mar. Chem.* **1990**, *28* 333-351.
19. Manuel Algarra Gonzalez and Miguel Hernandez Lopez, Determination of fluorene in sea-water by room temperature phosphorescence in organised media. *Analyst*. **1998**, 123, 2217–2221.
20. Donaldson, D.J.; Kahan, T.F.; Kwamena, N.-O.A.; Handley, S.R.; Barbier, C. In: Valsaraj, Kommalapati (Eds.). Atmospheric Chemistry of Urban Surface Films. *Am. Chem. Soc.* **2009**, 79-89.
21. Monge, M. E.; D'Anna, B.; Mazri, L.; Giroir-Fendler, A.; Ammann, M.; Donaldson, D. J.; George, C. Light changes the atmospheric reactivity of soot. *Proc. Natl. Acad. Sci. U. S. A.* **2010**, *107*, 6605-6609.
22. Styler, S. A.; Loiseaux, M. E.; Donaldson, D. J. Substrate effects in the photoenhanced ozonation of pyrene. *Atmos. Chem. Phys.* **2011**, *11*, 1243-1253.

23. Keyte, I. J.; Harrison, R. M.; Lammel, G. Chemical reactivity and long-range transport potential of polycyclic aromatic hydrocarbons – a review. *Chem. Soc. Rev.* **2013**, *42*, 9333-9391.
24. Zelenyuk A.; Imre, D.G.; Wilson, J.; Bell, D.M.; Suski, K.J.; Shrivastava, M.; Beránek, J.; Alexander, M.L.; Kramer, A.L.; Simonich, . S. L. The effect of gas-phase polycyclic aromatic hydrocarbons on the formation and properties of biogenic secondary organic aerosol particles. *Farad. Discuss.* **2017**, *200*, 143-164.
25. Zhou, S.; Hwang, B. C. H.; Lakey, P. S. J.; Zuend, A.; Abbatt, J. P. D.; Shiraiwa, M. Multiphase reactivity of polycyclic aromatic hydrocarbons is driven by phase separation and diffusion limitations. *Proc. Natl. Acad. Sci. U. S. A.* **2019**, *116*, 11658–11663.
26. Mekic, M.; Zeng, J.; Jiang, B.; Li, X.; Lazarou, Y. G.; Brigante, M.; Herrmann, H.; Gligorovski, S. Formation of toxic unsaturated multifunctional and organosulfur compounds from the photosensitized processing of fluorene and DMSO at the air-water interface. *J. Geophys. Res.: Atmos.* **2020**, doi:10.1029/2019JD031839.
27. Grossman, J. N.; Stern, A. P.; Kirich, M. L.; Kahan, T. F. Anthracene and pyrene photolysis kinetics in aqueous, organic, and mixed aqueous-organic phases. *Atmos. Environ.* **2016**, *128,* 158-164.
28. Kinani, S.; Soussi, Y.; Kinani, A.; Vujovic, S.; Aït-Aïssa, S.; Bouchonnet, S. Photodegradation of fluorene in aqueous solution: Identification and biological activity testing of degradation products. *J. Chromatogr. A*. **2016**, *1442*, 118-128.
29. Herrmann, H.; Schaefer, T.; Tilgner, A.; Styler, A. S.; Weller, C.; Teich, M.; Otto, T. Tropospheric Aqueous-Phase Chemistry: Kinetics, Mechanisms, and Its Coupling to a Changing Gas Phase. *Chem. Rev*. **2015**, *115*, 4259−4334.
30. Mekic, M.; Loisel, G.; Zhou, W.; Jiang, B.; Vione, D.; Gligorovski, S. Ionic strength effects on the reactive uptake of ozone on aqueous pyruvic acid: Implications for air-sea ozone deposition. *Environ. Sci. Technol.* **2018**, *52*, 12306–12315.
31. Mekic, M.; Brigante, M.; Vione, D.; Gligorovski, S. Exploring the ionic strength effects on the photochemical degradation of pyruvic acid in atmospheric deliquescent aerosol particles. *Atmos. Environ*. **2018,** *185*, 237-242.
32. Zhou, W.; Mekic, M.; Liu, J.; Loisel, G.; Jin, B.; Vione, D.; Gligorovski, S. Ionic strength effects on the photochemical degradation of acetosyringone in atmospheric deliquescent aerosol particles, *Atmos. Environ*. **2019,** *198*, 83-88.
33. Gómez Alvarez, E.; Wortham, H.; Strekowski, R.; Zetzsch, C.; Gligorovski, S. Atmospheric photo-sensitized heterogeneous and multiphase reactions: From outdoors to indoors. *Environ. Sci. Technol.* **2012**, *46*, 1955-1963.
34. Librando, V.; Bracchitta, G.; de Guidi, G.; Minniti, Z.; Perrini, G.; Catalfo, A. Photodegradation of anthracene and benzo[a]anthracene in polar and apolar media: new pathways of photodegradation. *Polycycl. Aromat. Compd.* **2014**, *34* (3), 263-279.
35. Mekic, M.; Liu, J.; Zhou, W.; Loisel, G.; Cai, J.; He, T.; Jiang, B.; Yu, Z.; Lazarou, Y. G.; Li, X.; Brigante, M.; Vione, D.; Gligorovski, S. Formation of highly oxygenated multifunctional compounds from cross-reactions of carbonyl compounds in the atmospheric aqueous phase, *Atmos. Environ.* **2019**, *219*, 1-12.
36. Zeng, J.; Yu, Z.; Mekic, M.; Liu, J.; Li, S.; Loisel, G.; Gao, W.; Gandolfo, A.; Zhou, Z.; Wang, X.; Herrmann, H.; Gligorovski, S.; Li, X. Evolution of indoor cooking emissions

captured by using secondary electrospray ionization high resolution mass spectrometry, *Environ. Sci. Technol. Lett.*, **2020**, *7*, 76-81.
37. Hughey, C. A.; Hendrickson, C. L.; Rodgers, R. P.; Marshall, A. G. Kendrick Mass Defect Spectrum : A Compact Visual Analysis for Ultrahigh-Resolution Broadband Mass Spectra. *Anal. Chem.* **2001**, *73* (19), 4676–4681.
38. Kourtchev, I.; Connor, I. P. O.; Giorio, C.; Fuller, S. J.; Kristensen, K.; Maenhaut, W.; Wenger, J. C.; Sodeau, J. R.; Glasius, M.; Kalberer, M. Effects of Anthropogenic Emissions on the Molecular Composition of Urban Organic Aerosols : An Ultrahigh Resolution Mass Spectrometry Study. *Atmos. Environ*. **2014**, 89, 525–532.
39. Liu, Y.; Sheaffer, R. L.; Barker, J. R. Effects of Temperature and Ionic Strength on the Rate and Equilibrium Constants for the Reaction Iaq + I-aq = I2-aq. *J. Phys. Chem. A* **2003**, *107*, 10296-10302.
40. Herrmann, H. Kinetics of Aqueous Phase Reactions Relevant for Atmospheric Chemistry. *Chem. Rev*. **2003**, *103*, 4691-4716.
41. Debye P.; Mc Aulay, J. Das elektrische Feld der Ionen und die Neutralsalzwirkung. *Physik. Zeitschr*. **1925**, *26*, 22-29.
42. Davies, C. W. Ion Association. Butterworths: North Ryde, Australia, **1962.**
43. Bao, Z-C.; Barker, J. R. Temperature and Ionic Strength Effects on Some Reactions Involving Sulfate Radical [SO_4^-(aq)]. *J. Phys. Chem*. **1996**, *100*, 9780-9787.
44. Guggenheim, E. A.; Wiseman, L. A. Kinetic Salt Effects on the Inversion of Sucrose. *Proc. R. Soc. Lond. A*. **1950**, *203*, 17-32.
45. Perlmutter-Hayman, B.; Stein, G. Specific Ionic Effects on Reaction Rates. The Reaction between Persulfate and Iodide Ions in the Presence of High Concentrations of Added Salts. *J. Chem. Phys.* **1964**, *40*, 848-852.
46. Clarke, A. G.; Radojevic, M. Chloride ion effects on the aqueous oxidation of SO_2. *Atmos. Environ*. **1983**, *17*, 617.
47. Lagrange, J.; Pallares, C.; Wenger G.; Lagrange P. Electrolyte Effects on Aqueous Atmospheric Oxidation of Sulphur Dioxide by Hydrogen Peroxide. *Atmos. Environ*. **1993**, *27A*, 129-137.
48. Umschlag, T.; Zellner, R.; Herrmann, H. Laser-based studies of NO3 radical reactions with selected aromatic compounds in aqueous solution. *Phys. Chem. Chem. Phys*. **2002**, *4*, 2975–2982.
49. Weller, C.; Hoffmann, D.; Schaefer, T.; Herrmann, H. Temperature and ionic strength dependence of NO_3-radical reactions with substituted phenols in aqueous solution. *J. Phys. Chem*. **2010**, *224*, 1261–1287.
50. Lin, P.; Rincon, A.G.; Kalberer, M.; Yu, J.Z. Elemental Composition of HULIS in the Pearl River Delta Region, China: Results Inferred from Positive and Negative Electrospray High Resolution Mass Spectrometric Data. *Environ. Sci. Technol*. **2012**, *46*, 7454−7462.
51. Wang, K.; Zhang, Y.; Huang, R-J.; Cao, J.; Hoffmann, T. UHPLC-Orbitrap mass spectrometric characterization of organic aerosol from a central European city (Mainz, Germany) and a Chinese megacity (Beijing). *Atmos. Environ*. **2018**, *189*, 22-29.
52. Rincon, A.G.; Calvo, A.I.; Dietzel, M.; Kalberer, M. Seasonal differences of urban organic aerosol composition – an ultra-high resolution mass spectrometry study. *Environ. Chem.* **2012**, *9*, 298-319.

53. Kawamura, K.; Gagosian, R.B. Implications of ω-oxocarboxylic acids in the remote marine atmosphere for photo-oxidation of unsaturated fatty acids. *Nature*. **1987**, *325*, 330-332.
54. Tao, S.; Lu, X.; Levac, N.; Bateman, A.P.; Nguyen, T.B.; Bones, D.L.; Nizkorodov, S.A.; Laskin, J.; Laskin, A.; Yang, X. Molecular Characterization of Organosulfates in Organic Aerosols from Shanghai and Los Angeles Urban Areas by Nanospray-Desorption Electrospray Ionization High-Resolution Mass Spectrometry. *Environ. Sci. Technol*. **2014**, *48*, 10993−11001.

55. Hopkins, R. J.; Desyaterik, Y.; Tivanski, A. V.; Zaveri, R. A.; Berkowitz, C. M.; Tyliszczak, T.; Gilles, M. K.; Laskin, A. Chemical Speciation of Sulfur in Marine Cloud Droplets and Particles: Analysis of Individual Particles from the Marine Boundary Layer over the California Current. *J. Geophys. Res.: Atmos*. **2008**, *113*, D04209.
56. Gaston, C. J.; Pratt, K. A.; Qin, X.; Prather, K. A. Real-time Detection and Mixing State of Methanesulfonate in Single Particles at an Inland Urban Location during a Phytoplankton Bloom. *Environ. Sci. Technol*. **2010**, *44*, 1566−1572.

57. Frank, R.; Klopffer, W. Spectral solar photo irradiance in Central Europe and the adjacent North Sea. *Chemosphere* **1988**, *17*, 985–994.